LIQUID AGENT TRANSPORT AROUND SOLID OBSTACLES

Cary Presser[†], John Widmann[†], and George Papadopoulos[‡]

[†]National Institute of Standards and Technology
Gaithersburg, MD 20899-8360

[‡]Dantec Dynamics
Mahwah, NJ 07430

ABSTRACT

The focus of this effort is to investigate the dispersal of liquid fire suppression agents around solid obstacles, and obtain a better understanding of the physical processes of droplet transport in cluttered spaces. An experimental investigation is presented to examine the flow field dynamics of highly turbulent flow over obstacles, and spray transport in such flow fields. The obstacles of interest were a cylinder and body-centered cube (BCC) arrangement of spheres. Transport of both water droplets and seed particles was characterized upstream and downstream of these obstacles using particle image velocimetry (PIV). Data were recorded for the cylinder at ambient temperature and after being heated to 423 K to estimate the effects of the hot cylinder surface on droplet transport. The results indicate that smaller droplets are entrained into the recirculation region behind the cylinder while the larger droplets impact the cylinder surface, accumulate, and drip off, or disperse radially away from the surface regardless of their interaction with the cylinder. The flow over the heated cylinder indicates the formation of layer of vaporizing liquid on the downstream side of the cylinder in the shear region between the recirculation zone and free stream. In addition, surface cooling that resulted from spray impingement was around 50 % of the preset cylinder temperature. For the BCC (with a blockage ratio of about 64 %), there is both transport of droplets and seed particles around and through the BCC, as well as significantly more liquid accumulation and dripping than for the cylinder.

INTRODUCTION

The new generation of Halon replacements include chemical suppressants that have high boiling point temperatures (*i.e.,* $T_b > 330$ K) and exist in liquid phase under high-pressure release or in ambient conditions. Release of these agents in a confined space results in the dispersal of droplets that either travel along ballistic trajectories, move with the convecting flow, or a combination of the two depending on the local Stokes number of the droplet. Therefore, an accurate representation of droplet transport is crucial for numerical modeling of fire suppression in confined spaces using these agents. To better understand the physics of droplet transport around and behind solid objects, an experimental arrangement at the NIST spray facility has been modified to impose controlled grid-generated turbulence on the air stream. Experimental results from this facility provide new experimental data for a well-characterized, homogenous droplet-laden turbulent flow field around prescribed obstacles. This experimental effort compliments another numerical effort to develop and validate the subgrid model of the VULCAN Computational Fluid Dynamics (CFD) fire physics code for spray-clutter interactive environments, under development at Sandia National Laboratories.

Baseline measurements of the discrete (spray) and continuous (gas) phase velocities with prescribed obstacles are reported in this study. This work is a continuation of a previous investigation on the measurement and numerical prediction of homogeneous turbulent flow over different diameter cylinders [1], which serves as a baseline for this droplet-laden flow study. The results were obtained using particle image velocimetry, and visualization techniques. Operating flow rates were based on typical engine-nacelle-like conditions. Liquid agent transport was investigated around two representative obstacles - a cylinder (having a diameter larger than the characteristic length-scale of turbulence), and a body-centered cubic arrangement of spheres. The cylinder represents a classical configuration and the body-centered cube represents a more complicated scenario. The cylinder was also heated to explore thermal effects on droplet vaporization and transport around the cylinder. These data will be used for subgrid model validation of the VULCAN fire physics code. This paper presents a description of the experimental arrangement and diagnostics used to characterize the droplet-laden flow field. The experimental results from the nonheated and heated cylinder, and body-centered cube are compared and discussed, along with comments on future work.

EXPERIMENTAL ARRANGEMENT

In order to explore droplet transport around obstacles, an experimental arrangement is used that provides a well-characterized homogeneous turbulent flow field around prescribed obstacles, and is shown in Fig. 1. The experimental setup includes a nonswirling air that coflows around the liquid agent injector. The experiment is oriented horizontally, as opposed to the original vertical arrangement (see Ref. 1), to enable collection of liquid agent that drips off of the obstacle, and prevent liquid droplets downstream of the obstacle from falling back upstream into the oncoming stream. The agent used in this study was water that was supplied to the flow field with a 60^{o} hollow-cone pressure-jet atomizer (with a nominal flow rate of 3.78 kg/h). An octagon-shaped Plexiglas insert (with a wall thickness of 6 mm, length of 610 mm, and major and minor axes of 760 mm and 560 mm) was used as a boundary condition. The Plexiglas insert, along with the front face that supported the inlet passages for the liquid agent and air, and back face that supported the exhaust passage, served to form a closed system. A honeycomb layer (51 mm thick with 3 mm size cells) is used to straighten the airflow, which is co-positioned around an injector for the agent. Grid-generated turbulence is imposed on the air stream by placing a square layer of wire mesh screen (with dimensions of 229 mm by 330 mm, and 13 mm size cells) downstream of the honeycomb. For these experiments, the incoming air (supplied from a 7 L/min compressor) was directed entirely through a distributor plate with steel wool, circular cross sectional area of the honeycomb (203 mm in diameter), and then through wire mesh screen (placed 25 mm downstream of the honeycomb), as shown in Fig. 1. The face of the liquid atomizer was placed flush with the upstream side of the grid, and centered within one mesh cell so that the liquid spray would be unimpeded by the grid. The integral and Kolmogorov length scales of turbulence are estimated to be 3 cm and 100 μm, respectively. A stepper-motor-driven traversing system translates the entire assembly, and permits measurements of the flow field properties at selected locations downstream of the injector.

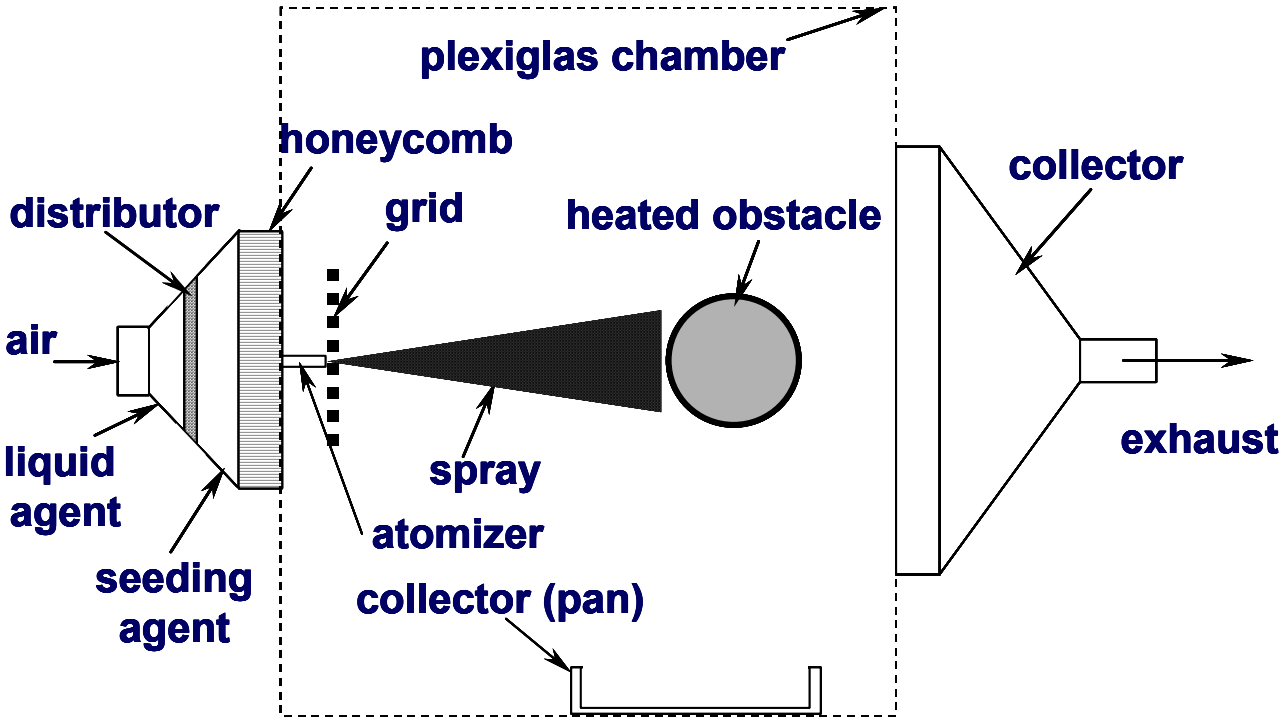

Figure 1. Schematic of the experimental arrangement for the droplet laden grid-generated turbulent flow field.

Measurements were carried out with two obstacles, an aluminum cylinder and a body-centered cube arrangement of wooden spheres (see Figs. 2 and 3, respectively). The cylinder used in this study has a diameter of 32 mm, which was chosen because its diameter is larger than the integral length scale of turbulence (see Ref. 1). The cylinder is an aluminum rod with a length of 305 mm (see Fig. 2). A hole (13 mm in diameter) was bored through the center for placement of a 250 W cartridge heater (13 mm in diameter and 76 mm in length). The rod was also cut into two halves and 1 mm deep channels bored along one segment for placement of five K-type thermocouples. The thermocouples have an inconel sheath, ungrounded, and 0.8 mm in diameter (305 mm long). The thermocouples were placed in a cross pattern in the center of the rod (each separated by a distance along the surface of 6.4 mm, with their tips (thermocouple junctions) placed about 3.2 mm of the surface with bored holes at each location). The central thermocouple was used for temperature control of the heater, which was positioned behind the thermocouples. The BCC is composed of nine wooden spheres with a nominal diameter of 28 mm, all interconnected with posts (with a nominal length of 24 mm and width of 3.2 mm) as shown in Fig. 3. (The posts connecting the center sphere were nominally 17 mm in length.) The blockage ratio, or obstructed cross-sectional area for an equivalent area encompassing a face of the BCC, was about 64 %. The two obstacles were coated with flat black paint to reduce reflections of laser light off their surface for any optical measurements. The obstacles were placed nominally 182 mm downstream of the honeycomb, and centered with the atomizer centerline. Choice of location of the screen and obstacles is discussed further in Ref. 1.

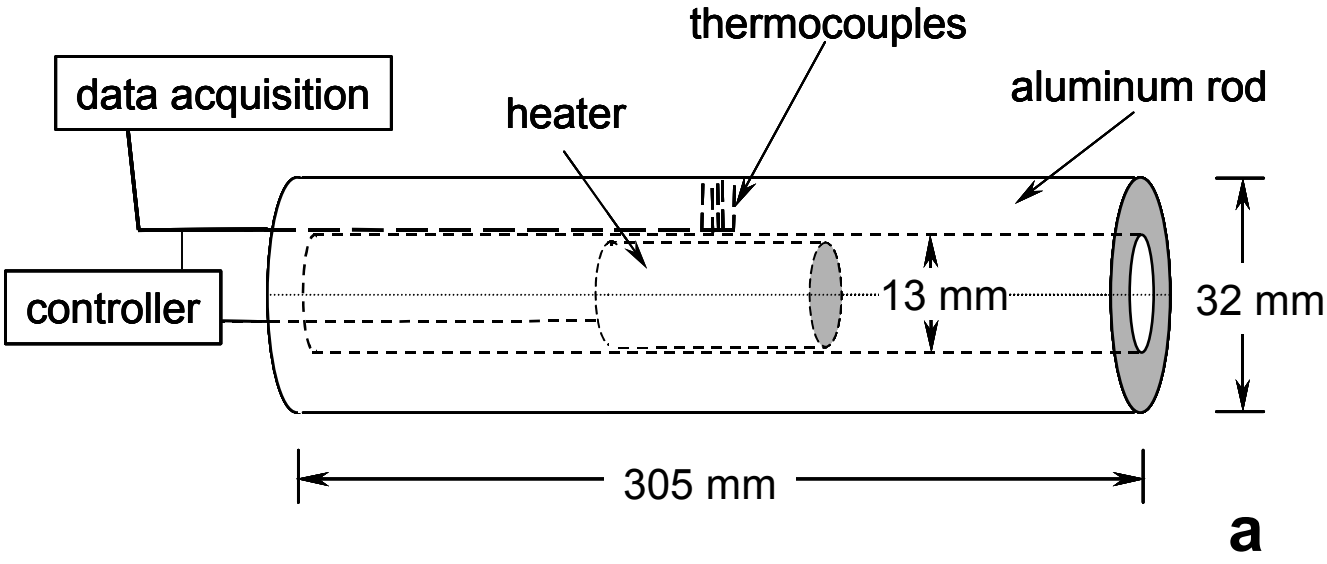

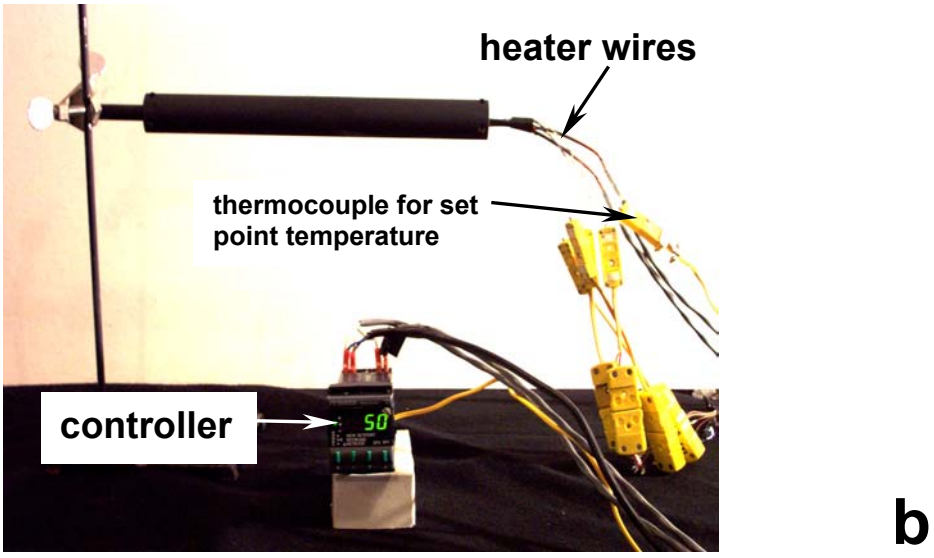

Figure 2. Experimental arrangement for the heated cylinder: a) schematic and b) front view.

The flow field was characterized using a three-dimensional particle image velocimetry (PIV) system from Dantec Dynamics* (see Fig. 4). PIV is a non-intrusive field measuring technique (as opposed to a single-point diagnostic method) that can measure two or three components of velocity. The method requires seed particles to be added to the flow, which are then assumed to follow the streamlines and act as tracers. The spatial displacement of the seed particles, corresponding to two images separated by a known time period (the time between laser pulses was 70 μs), is measured and the velocity is deduced. The pencil fogger generates water-based seed particles approximately 1 μm in diameter. A separate supply of air (negligible with regard to the total compressor air flow supplied to the experiment) was used to carry the fog aerosol from an enclosed aluminum

*Certain commercial equipment or materials are identified in this publication to specify adequately the experimental procedure. Such identification does not imply recommendation or endorsement by the National Institute of Standards and Technology, nor does it imply that the materials or equipment are necessarily the best available for this purpose.

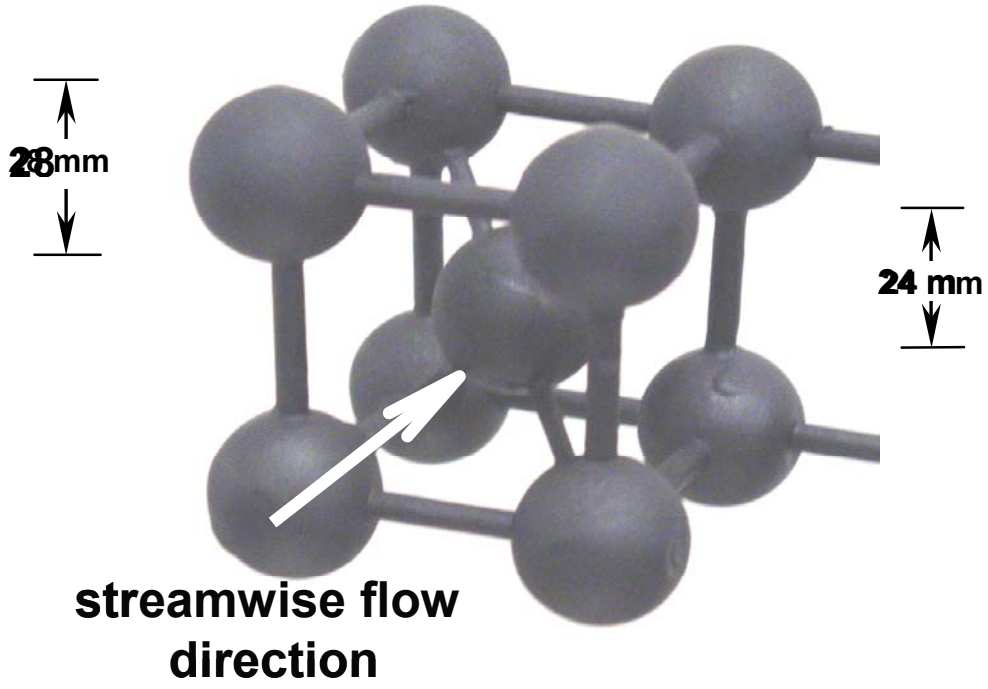

Figure 3. View of the body-centered cube of spheres.

box containing the fogger into the main air stream downstream of the distributor plate (see Fig. 1). A tube with several holes was stretched across the passage to enable dispersion of the fog seed across the measurement area. The PIV images are obtained in a plane corresponding to the laser light sheet, which is oriented downward from above the Plexiglas chamber and onto a cross section of the obstacle.

The 3-D stereo PIV system differs from traditional PIV systems in that two CCD cameras are used, and three velocity components are measured [2]. A 50 mJ Nd:YAG laser was used as the illumination source for the PIV measurements. The pulse duration of the laser light sheet was about 5 ns, and the wavelength of the light was 532 nm. A pair of 12-bit double-frame CCD cameras with a resolution of 1024 x 1280 pixels was used to obtain the images. Special camera mounts were utilized to permit the rotation of the camera body with respect to the camera lens so the Scheimpflug condition was satisfied, permitting the laser sheet to be in focus despite the non-orthogonal camera alignment [2]. Bandpass filters (center wavelength = 532 nm, acceptance window = 30 nm) were used to reject the broadband white light from the room. The two cameras were placed at angles of about 95^{o} and 145^{o} from the vertical orientation of the laser beam, i.e., as measured from the forward direction of propagation of the laser sheet. The processed results are presented as a composite mapping of individual planar regions that are about 33 mm in height and 53 mm in width (i.e., field of view for common overlap region of both cameras). Statistics were obtained from about 500 - 700 individual records (obtained at a rate of approximately 3 Hz). Each field of view represents about 9900 vectors for the seeded-only flow, and 4950 vectors for the spray-only case. The spatial resolution of the measurements depends directly upon the pixel interrogation area (i.e., 16 x 16 pixels, with a pixel size/resolution of 6.7 μm), resulting field of view, total number of pixels, and laser light sheet thickness (i.e., 2 – 3 mm), and indirectly on the seeding density. Using only seed particles, the spatial resolution was approximately 700 μm in the plane of the

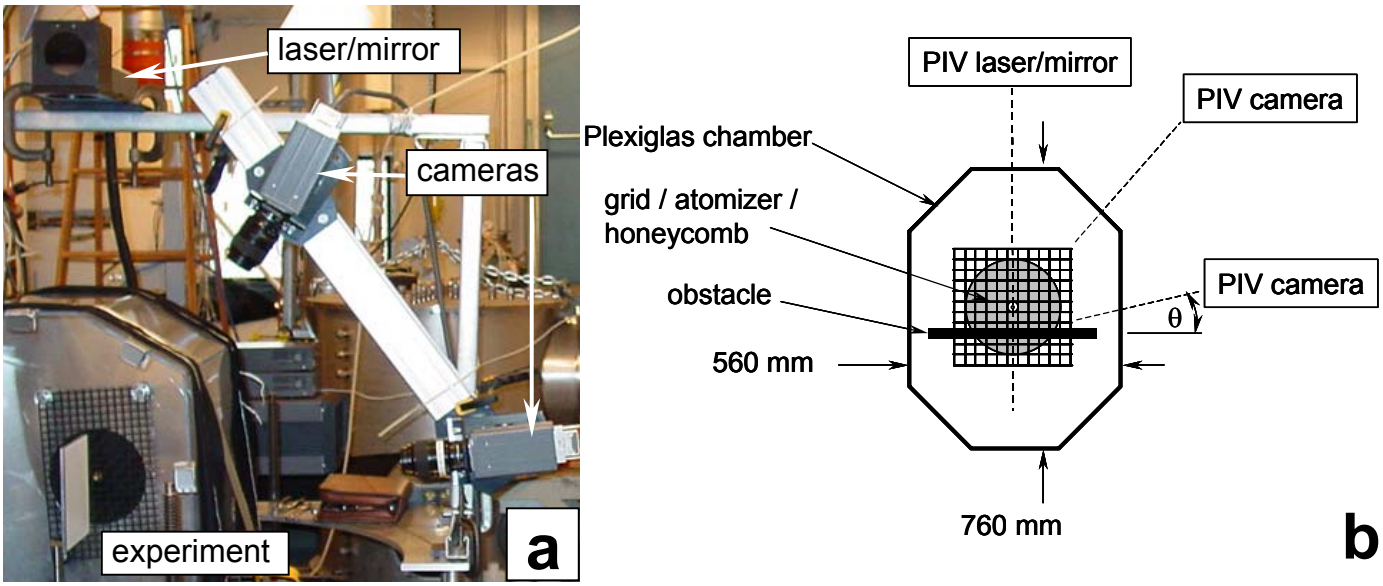

Figure 4. View and schematic of the experimental arrangement with the cameras and laser from the PIV system.

laser sheet (for the spray only, the resolution was about 1.5 mm due to the lower droplet concentration and larger droplet sizes). The velocity resolution was about 5 mm/s.

Measurements of the flow field were carried out along the centerline of the measurement area for the cylinder and BCC. Also, two additional off-axis planes were interrogated to map out one quadrant of the BCC, i.e., 1) between the center and two outer spheres, and 2) slightly outside of the center of the two outer spheres. For the cylinder, three cases were recorded, i.e., 1) with seed only, 2) with droplets only, and 3) with both seed and droplets, in order to try to isolate the effects of the droplets/particles on the flow field dynamics.

RESULTS AND DISCUSSIONS

FLOW FIELD VISUALIZATION

The droplet-laden flow field over each obstacle was recorded with a digital movie camera at 9 frames/s. Examples of the observed droplet/particle transport processes are shown in Fig. 5 for a) seeded only and b) droplet only flow over the unheated cylinder, and c) combined droplet and seeded flow over the BCC. The seed is entrained in the turbulent flow field (see Fig. 5a) and a relatively high concentration of particles is observed in the wake behind the cylinder [3]. On the other hand, the droplets in the center of the spray are found to impinge on the surface of the cylinder while those droplets at larger radial positions flow around or past the cylinder with an increased radial component of velocity (see Fig. 5b). Few droplets are observed behind the cylinder in its wake. Droplets that impinge and wet the cylinder surface drip off at a rate of approximately one drop every 5 s. The seed (fog smoke) was observed to leave a residue on the upstream side of the cylinder. There was no evidence of secondary breakup of the droplets, which was expected because the Weber number (*We*) was too low ($We \cong 140$ for a 500 μm diameter water droplet, whereas the critical Weber number for droplet shattering is approximately

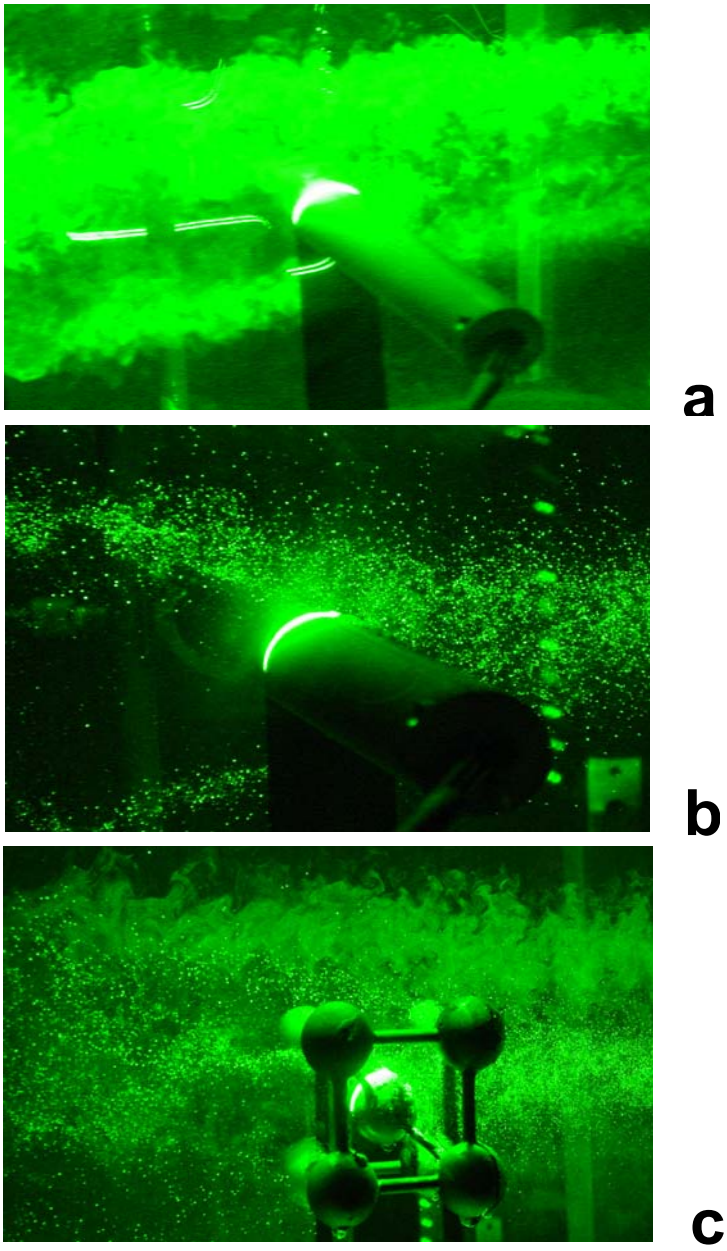

Figure 5. Photographs of the a) seed/droplet-laden flow field around the unheated cylinder, b) droplet-laden flow field around the unheated cylinder, and c) seed/droplet-laden flow field around the body-centered cube of spheres. Flow direction is from right to left.

two orders of magnitude larger) [4]. When the cylinder was heated to 423 K, the spray cooled the cylinder down to 351 K. The droplet-laden flow over the cylinder appeared to be similar to the unheated case except along the shear layer downstream of the cylinder. In this region, a vapor layer formed which was presumed to be the result of vaporization of the liquid that wet the hot surface.

The transport of droplets through the BCC (see Fig. 5c) is interesting in that both the spheres and connecting rods (that act like cylinders) block the droplets, while the flow field traversing through the obstacle will also provide a path for the entrained droplets (recall that the nominal blockage ratio is about 64 %). Dripping is observed from each

sphere at a rate of approximately 1 droplet/s. If one assumes that droplets fall off each sphere at this rate, one can determine that this liquid represents approximately 4.5 % of the inlet water flow (assuming a dripped droplet diameter of 8.5 mm, which was an estimated largest droplet size observed from digital movies). Although the BCC has more dripping of liquid than the cylinder, the major portion of the spray is still able to traverse the obstacle.

DROPLET/PARTICLE VELOCITIES MEASUREMENTS

Particle image velocimetry (PIV) was used to obtain instantaneous two-dimensional images of the air flow field velocity (*i.e.*, three components of velocity). These images were then used to construct profiles of the streamwise (W) and two cross-stream (U – spanwise along the cylinder length, and V – upward vertically from the cylinder) mean velocities, turbulence intensity (T_i, where $i = U, V, W$), and velocity correlation coefficients (ρ, from which the Reynolds stresses can be derived), both upstream and downstream of the cylinder, and along the central plane that is referenced by the position of the atomizer. Although the orientation of the Plexiglas chamber was different than in our earlier study [1], and an atomizer was incorporated into this configuration, little difference was found in the homogeneous turbulent flow field. The maximum gas streamwise component of velocity was $W \cong 4.0$ m/s (Reynolds number of about 3300, based on the grid cell size), and the maximum turbulence intensity was $T_W \cong 7.5$ %. Note that these values are slightly smaller than reported earlier because obstacles were placed approximately 75 mm further downstream than in our previous study in order to reduce the influence of the jetting from the grid (see Ref. 1).

The three components of droplet velocity for the flow over the unheated cylinder are presented in Fig. 6. In the figure, three cases are presented that represent the flow with the seed only, both seed and spray, and spray only. The black circle represents the position and size of the cylinder. The black contours lines represent stream traces (i.e., direction) of the in-plain V-W velocity vectors. The seed only case compares with our earlier study of the fluid flow over different size cylinders (see Ref. 1). The flow pattern is, as expected similar to the previous study. The free stream air velocity reaches a streamwise value of $W \cong 4.5$ m/s around the side of the cylinder, and the flow behind each cylinder forms a recirculation region ($W \cong -1.0$ m/s). The reverse flow behind the cylinders appears to extend about two cylinder diameters downstream. The turbulence intensity increases behind the cylinders ($T_W \cong 30$ %) in a shear region behind the obstacle. There is a significant correlation of the velocity fluctuations downstream of the cylinder between the streamwise and V-cross-stream components (an absolute value of 0.7 is reached for the correlation coefficient, similar to what was reported in Ref. 1). This result is indication of the shear between the free stream and reverse flow region behind the cylinder. The flow also decelerates to a stagnation region along the centerline at the upstream face of the cylinder. The V-component of velocity increases significantly around the side of the cylinder indicating the radial displacement and separation of the droplets, seed, and fluid flow. Comparison of the two cases with spray to the seed-only case indicates that the recirculation zone is somewhat larger for the spray cases. Larger

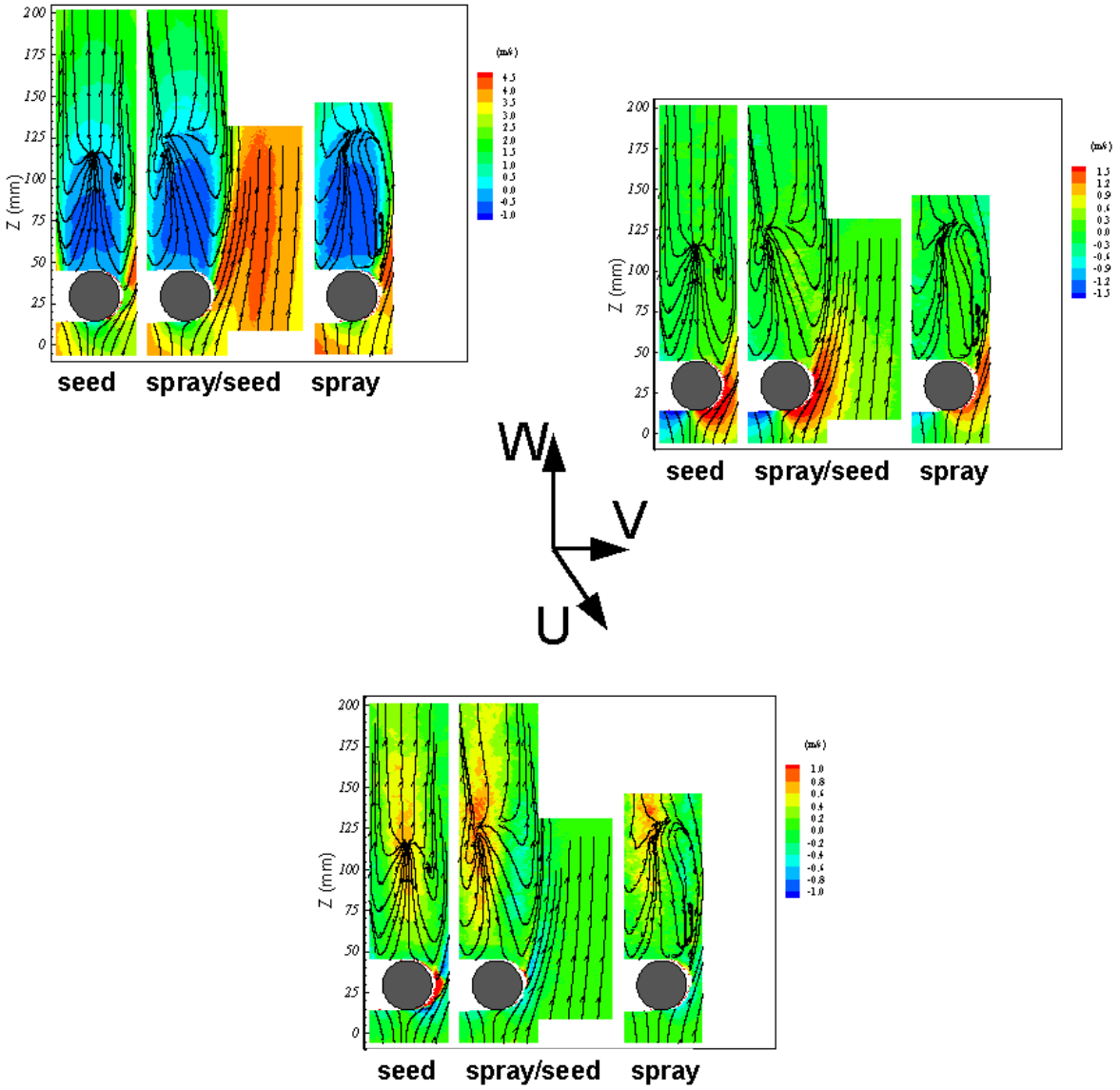

Figure 6. Variation of the mean streamwise and cross-stream velocities with downstream distance for the unheated cylinder. Contours are the stream traces of the in-plane vectors obtained from the axial and radial components of velocity.

size droplets require a longer distance to interact with the turbulent flow field, reduce their higher momentum, and be entrained into the recirculation zone.

The stream trace (contour lines) also shows an unexpected pattern behind the cylinder near the stagnation point. Instead of presenting closed loops that indicate a recirculating pattern, the contours appear to emanate from the stagnation region. One possible explanation is that in the stagnation region the *U*-component of velocity reaches an absolute value of nearly 0.8 m/s, indicating a strong spanwise flow along the length of the cylinder in both directions. Spanwise flow is also found on the upstream side face of the cylinder. It appears to be generated by the cylinder and may be related to the finite cylinder length (with an aspect ratio of about 10:1) [5]. The droplet-laden flow over

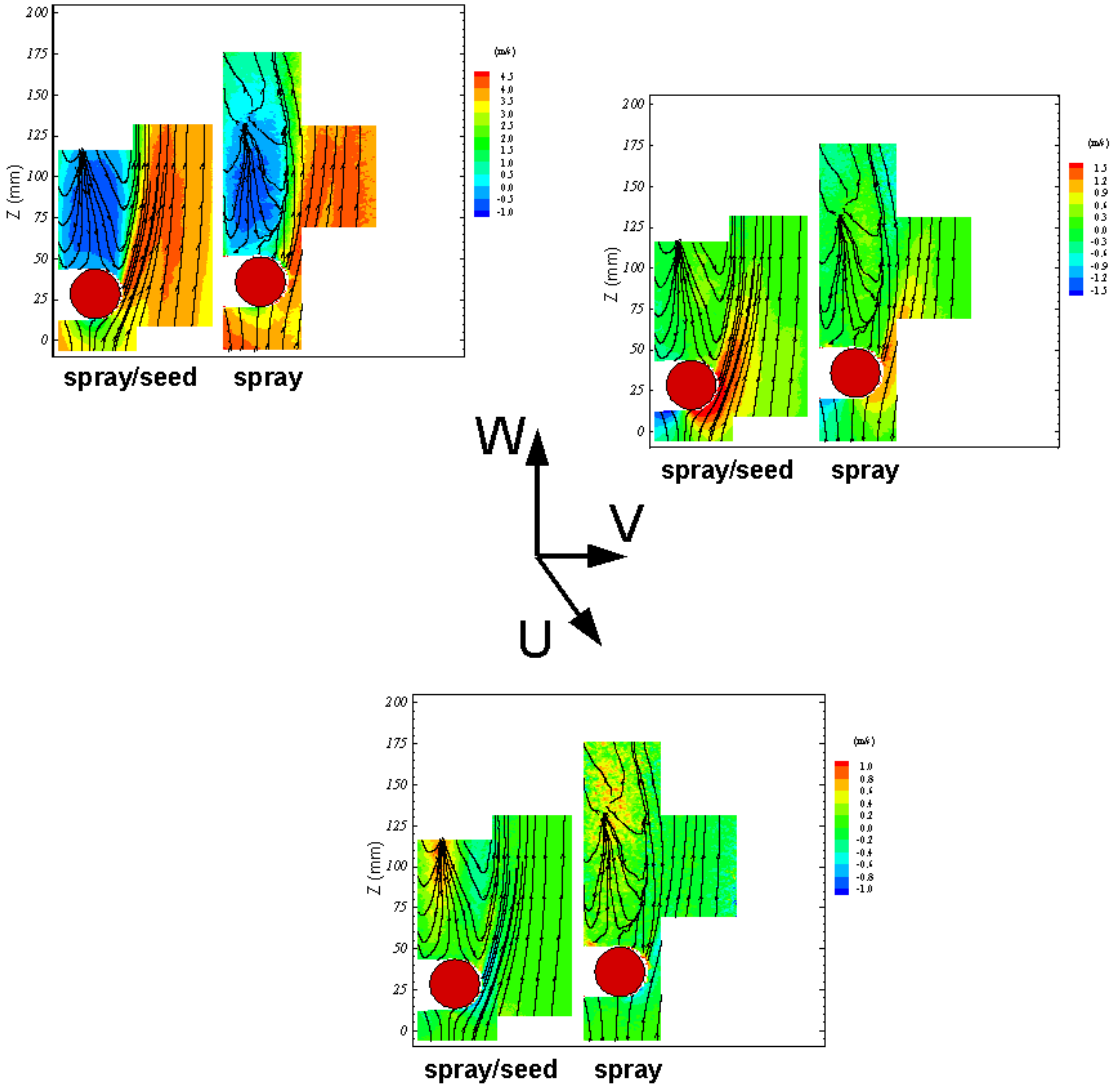

Figure 7. Variation of the mean streamwise and cross-stream velocities with downstream distance for the heated cylinder. Contours are the stream traces of the in-plane vectors obtained from the axial and radial components of velocity.

the heated cylinder, presented in Fig. 7, is similar to the unheated cases (only the spray and combined spray/seed cases are presented). Differences between the heated and unheated cases are found for the spray-only case: 1) a stronger streamwise flow and weaker reverse flow behind the cylinder (see *W*-component of velocity), 2) a weaker radial flow around the side of the cylinder (see *V*-component of velocity), and 3) the *U*-component cross-stream flow is further downstream of the cylinder. The result is that the hot cylinder is developing a more streamwise droplet-laden flow near the cylinder. Figure 8 presents velocity field around the BCC for the combined spray/seed case. Although the configuration is more complicated, there are still similar features to the cylinder case. The flow accelerates around the spheres and there is reverse flow in the wake region. In addition, the presence of cross-stream component of the flow is evident around the spheres. This cross flow may be a result of the three-dimensional nature of the spheres and flow field, and the transport of entrained droplets and seed through convoluted pathways of this obstacle.

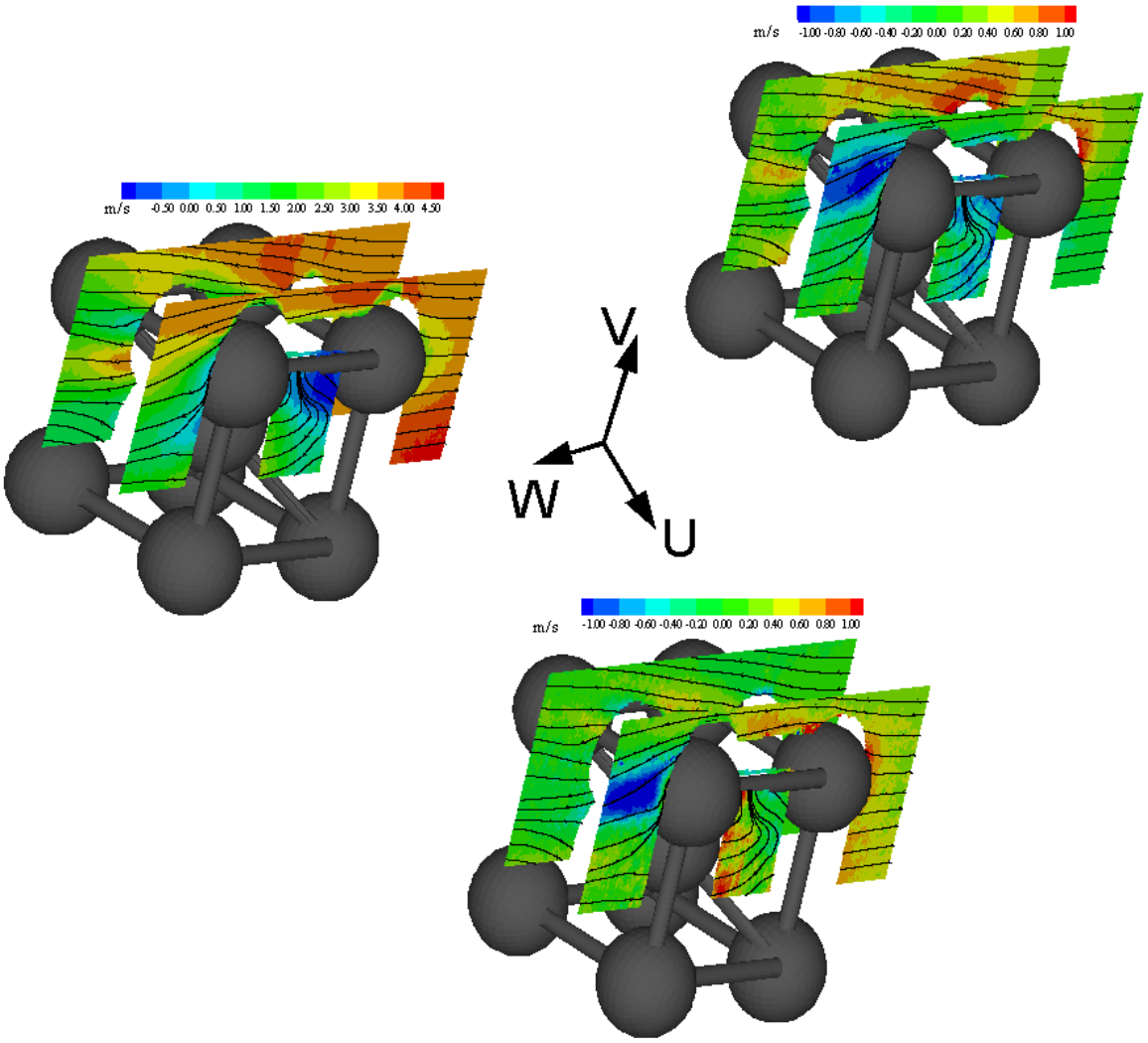

Figure 8. Variation of the mean streamwise and cross-stream velocities with downstream distance for the body-centered cube of spheres. Contours are the stream traces of the in-plane vectors obtained from the axial and radial components of velocity.

NEXT PHASE

This experimental work will study next droplet transport processes of another liquid fire suppressant agent in the regions upstream and downstream of different obstacle configurations. The liquids that will be used are water and HFE-7100 (boiling point of 334 K) because of the effectiveness of high boiling point liquids to extract heat from a flame zone. A two-component phase Doppler interferometry system will be used to obtain spatial profiles of the droplet size and velocity distributions, and droplet number density, and allow comparison of water and HFE-7100 in order to study the effects of different physical properties on droplet transport. If needed, PIV measurements will be carried out to provide the spray and flow field characteristics upstream and downstream of obstacles under different operating conditions. The results will be used to provide data for input and validation for the subgrid turbulence model of the VULCAN fire code.

CONCLUSIONS

Particle image velocimetry measurements were carried out for a droplet-laden, homogeneous turbulent flow over an unheated and heated cylinder, and body-centered cube arrangement of spheres. Droplets were observed to impact the cylinder surface and either wet (leading to dripping) or rebound off the surface. The Weber number was too low to lead to droplet shattering. Significant spray cooling of the surface and the presence of a vapor stream downstream of the cylinder along the shear layer was observed for the heated cylinder. Comparison of the velocity fields obtained with water droplets from a pressure-jet atomizer and 1 μm size seed particles formed from a fogging device indicate that dispersion of droplets/particles around an obstacle is dependent on its size. Future efforts of this work will be directed to investigating other liquid agents (i.e., HFE-7100) to determine physical property effects on transport processes. Also, these results provide a baseline for future comparison with simulations from the Vulcan fire code under development at Sandia National Laboratories.

ACKNOWLEDGEMENTS

The authors wish to acknowledge the partial support of this research by the Department of Defense Next Generation Fire Suppression Technology Program, funded by the DoD Strategic Environmental Research and Development Program. The authors wish to thank P. DesJardin, L. Gritzo, D. Keyser, P. Disimile, and J. Tucker of the NGP Project 6A/1 on development of a spray-clutter interaction model for the discussions and guidance that they have provided us, Mr. R. Fink for his technical assistance in completing the NIST facility modifications.

REFERENCES

1. Presser, C., Widmann, J.F., DesJardin, P.E., and Gritzo, L.A., "Measurements and Numerical Predictions of Liquid Agent Dispersal Around Solid Obstacles," Proc. Halon Options Technical Working Conf. (HOTWC-2001), pp. 122-130, New Mexico Engineering Research Institute, Albuquerque, NM, 2001.

2. Flowmap® 3D-PIV System Owner's Manual, Dantec Measurement Technology, Inc., Mahwah, NJ, July 1999.

3. Wang, G., Bachalo, E.J., Sankar, S.V., and Bachalo, W.D., "An Investigation of Spray Interaction with Large-Scale Eddies, " Proc. 5th Annual Conf. on Liquid Atomization and Spray Systems (ILASS Americas '92), pp. 53-58, San Ramon, CA, 1992.

4. DesJardin, P.E., Presser, C., Disimile, P.J., and Tucker, J.R., "A Droplet Impact Model for Agent Transport in Engine Nacelles," Proc. Halon Options Technical Working Conf. (HOTWC-2002), on CD, New Mexico Engineering Research Institute, Albuquerque, NM, 2002.

5. Williamson, C.H.K., "Oblique and Parallel Modes of Vortex Shedding in the Wake of a Circular Cylinder at Low Reynolds Numbers," J. Fluid Mech., Vol. 206, pp. 579-627 (1989).